

Systematic Coupled Cluster Study of Noncovalent Interactions Involving Halogens, Chalcogens, and Pnicogens

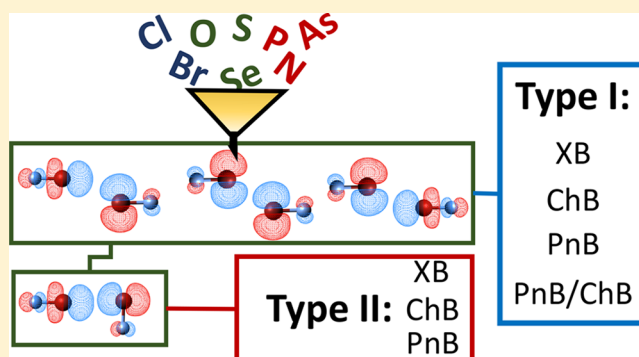
Published as part of *The Journal of Physical Chemistry virtual special issue “Manuel Yáñez and Otilia Mó Festschrift”*.

Vytor Oliveira and Elfi Kraka*[✉]

Computational and Theoretical Chemistry Group (CATCO), Department of Chemistry, Southern Methodist University, 3215 Daniel Ave, Dallas, Texas 75275-0314, United States

Supporting Information

ABSTRACT: The noncovalent interactions of 32 complexes involving pnicogens, chalcogens, and halogens atoms were investigated at the CCSD(T)/aug-cc-pVTZ level of theory. Two different types of complexes could be distinguished on the basis of geometric parameters, electron difference densities, and the charge transfer mechanisms associated with each type. In the type I conformation, the monomers adopt a skewed orientation allowing charge to be transfer between both monomers, whereas in the type II conformation the monomers adopt a linear arrangement, maximizing charge transfer in only one direction. Type I complexes involving the interaction between pnicogens and chalcogens cannot be unambiguously defined as chalcogen or pnicogen bonds, they are an admixture of both. The charge transfer dependence on the conformation adopted by the complexes described in this work can serve as a novel conformationally driven design concept for materials.



1. INTRODUCTION

The study of intermolecular interactions is an important topic in chemistry due to the key roles these interactions play in diverse fields. In supramolecular chemistry they can guide self-assembly¹ and stabilize the tertiary structures of macromolecules such as proteins, DNA, and RNA;^{2,3} In drug design they can lead to drug-receptor recognition.^{4,5} In catalysis they can help to stabilize the transition state of chemical reactions and guide stereoselectivity^{6,7} to name just a few examples. Although hydrogen bonding (HB) continues to be the most studied noncovalent interaction, there has been a continuous discovery of other kinds of weak interactions,^{1,8–13} which share many similarities with HB, such as high directionality^{14–16} and tunable interaction strength.^{17–24} Different types of interactions can possess unique electronic features relevant for the development of novel materials with special electrical,²⁵ magnetic,^{26,27} and optical properties.^{28–30} Among these new types of interactions, the ones involving pnicogen, chalcogen, and halogen atoms are already being exploited for the design and synthesis of liquid crystals, gels, molecular compartments,^{31,32} molecular linkers,³³ ion transport, sensors, optically responsive materials,³⁴ and novel drugs.^{35,36} These and other applications were the topic of recent reviews.^{1,37–42}

A well established example of such a noncovalent interaction that is known to play a determining role in the supramolecular structures and properties of crystals is the interaction between

two halogens (halogen...halogen).^{43–46} X-ray diffraction studies⁴⁷ supported by statistical analysis of crystal structures deposited on the Cambridge Database^{45,48} revealed that two preferred conformers are associated with halogen...halogen interactions. These are shown in Figure 1. In the type I

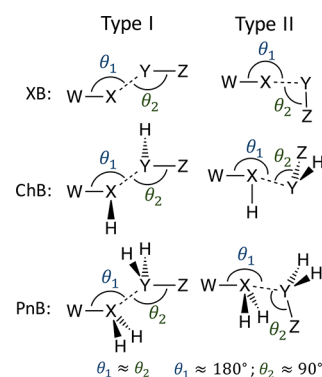


Figure 1. Representation of the two possible conformers involving halogen (XB), chalcogen (ChB), and pnicogen bonding (PnB) considered in this work.

Received: October 14, 2017

Revised: November 18, 2017

Published: November 20, 2017

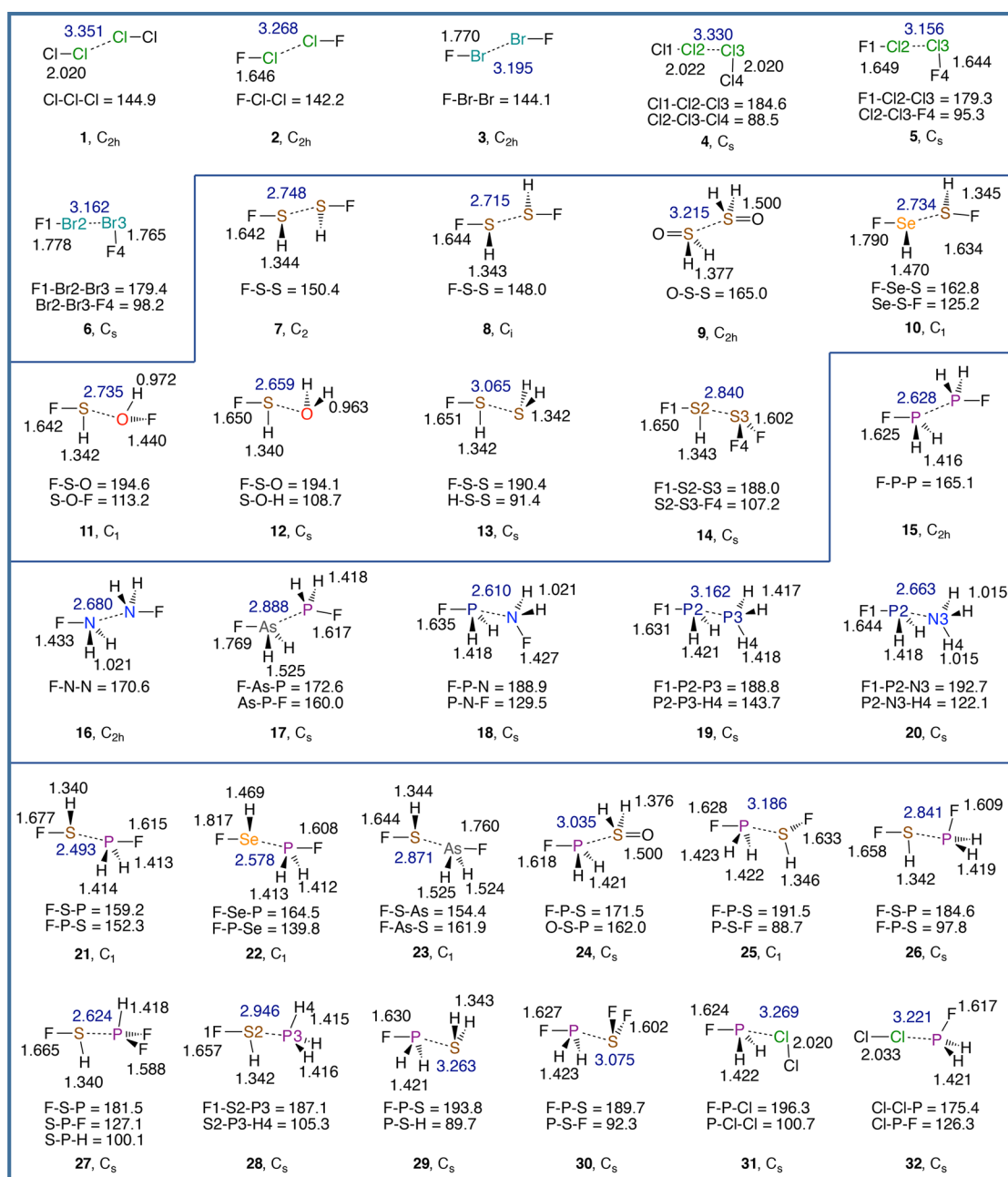


Figure 2. Schematic representation of the geometry of complexes 1–32. Bond distances in Å (intermolecular distances in blue) and selected angles in degrees.

conformation the two angles formed by the halogens X and Y and their substituents W and Z ($\theta_1 = \text{W}-\text{X}-\text{Y}$ and $\theta_2 = \text{X}-\text{Y}-\text{Z}$) have approximately the same value ($\theta_1 \approx \theta_2$), whereas type II contacts are characterized by a linear angle $\theta_1 \approx 180^\circ$ and a close to right angle $\theta_2 \approx 90^\circ$. Experimental and theoretical evidence suggests that type I halogen...halogen interactions are predominantly stabilized by dispersive forces.^{46,49,50} However, covalent contributions in the form of electron delocalization (i.e., charge transfer) from the lone pair X (lp(X)) orbital into the empty $\sigma^*(\text{YZ})$ orbital and from lp(Y) into the $\sigma^*(\text{WX})$ orbital⁴⁹ and electrostatic attraction, originating from the anisotropic distribution of the X and Y electron density,⁵¹ can also play a significant role for the stabilization of type I conformation. On the other hand, type II halogen...halogen interactions are considered to form true halogen bonds XB⁵²

(in the following XB is used for both type I and II halogen...halogen interactions for the sake of simplicity), as a result of the attractive interaction between the nucleophilic region of the halogen (Y) and the electrophilic region of the halogen (X) (Figure 1). Although type II XBs (XB-II) are generally stronger than the type I (XB-I), the latter are commonly observed due to crystal packing effects.^{46,53}

A different picture emerges for the closely related chalcogen...chalcogen and pnictogen...pnictogen interactions. Well-defined pnictogen bonds (PnBs) and chalcogen bonds (ChBs) are found for both type I^{12,23,54–61} and type II^{23,54,60,62,63} conformations (Figure 1). These are stabilized mostly by charge transfer and electrostatic contributions rather than by dispersion. Despite the many investigations on PnB and ChB exploring both type I and type II conformations, a

systematic comparison of XB, PnB, and ChB type I and type II conformations is still missing. Another topic of interest is the noncovalent interaction formed by atoms of different groups such as pnictogen...halogen or pnictogen...chalcogen, where multiple local minima involving different types of noncovalent interactions can be found. An example is the $\text{Cl}_2\cdots\text{PFH}_2$ complexes studied by Del Bene, Alkorta, and Elguero,^{64,65} involving three different types of $\text{Cl}\cdots\text{P}$ interactions, referring to a classical XB, a chlorine shared XB, and a PnB. Another interesting case is the complex $\text{FHSe}\cdots\text{PH}_2\text{F}$ studied by Shukla and Chopra,⁶⁶ which involves not only charge transfer (CT) from the phosphorus lone pair orbital ($\text{lp}(\text{P})$) into the $\sigma^*(\text{SeF})$ orbital of FHSe , characteristic of a ChB, but also the CT from $\text{lp}(\text{Se})$ to $\sigma^*(\text{PF})$, characteristic of a PnB, making it difficult to unambiguously classify the interactions as PnB or ChB.

A reliable comparison of the different kinds of interactions involving halogens, chalcogens, and pnictogens considering both type I and type II conformations, requires a method of high accuracy being capable to describe dispersive, electrostatic and covalent contributions in a well-balanced and accurate way. Although density functional theory with empirical dispersion corrections (DFT-D) and MP2⁶⁷ have been employed in various studies of noncovalent interactions, leading in general to a reasonably accurate description of HB, ChB, PnB, and XB, the reliability of these methods is challenged, when very weak noncovalent interactions have to be described.^{68–70} A more reliable choice in this case, especially when second or higher order properties are required, is the coupled cluster method with singles, doubles, and perturbative triples excitations (CCSD(T)).⁷¹ Considered as the current gold standard,⁷² CCSD(T) is usually the method of choice to evaluate the reliability of less computationally demanding approaches,^{73,74} and it is a particularly invaluable method in high-accuracy studies of small complexes.^{75,76}

In previous work⁷⁶ we presented for the first time a quantitative description of the intrinsic strength of 36 XB complexes in comparison with 8 HB, ChB, and PnB systems (all of type II conformation) by combining vibrational spectroscopy and high-accuracy CCSD(T) calculations. In the present study we will use a diverse set of 32 complexes consisting of XB, ChB, and PnB of both type I and type II conformations (shown in Figure 2) to explore the similarities and differences between the bonding mechanisms, the nature of the interactions, the intrinsic bond strength, and the influence of the atoms involved in the noncovalent interactions. For this purpose, we have addressed the following questions: (i) Is there a general mechanism to describe the noncovalent interactions formed by pnictogens, chalcogens, and halogens? (ii) Can we use other parameters besides the geometry to characterize the complex as been of type I or type II? (iii) How do the nature and the strength of the interaction depend on the atoms involved and on the conformation adopted? (iv) Is there any complex where type I and type II conformations are both minimum-energy points in the potential energy surface?

The paper is arranged as follows. In section 2 we provide details about the computational methods employed. In section 3 we describe the bonding mechanisms observed for type I and II conformations and discuss the most important factor involved in the stabilization of the complexes and in the intrinsic strength of the noncovalent interactions. In the last section we summarize the most important result and draw conclusion.

2. COMPUTATIONAL METHODS

The geometry of all complexes (1–32) and monomers (33–48) was fully optimized at coupled cluster level using CCSD(T)⁷¹ combined with Dunning's augmented triple- ζ basis sets aug-cc-pVTZ,^{77–79} which contains diffuse basis functions for a proper description of the density far from the nuclei. For the geometry optimizations the convergence criteria was set to 10^{-6} hartree bohr⁻¹ and a threshold of 10^{-9} was used for the self-consistent field and coupled cluster amplitude equations. Analytical vibrational frequencies computed at the same level were used to verify that each stationary point obtained from the geometry optimization is a minimum (or a first-order saddle point as in the case of complexes 1, 2, 3).

The Konkoli–Cremer method^{80–83} was used to convert the normal vibrational modes into local modes. This method makes use of a mass-decoupled analogue of Wilson equation of vibrational spectroscopy^{81,84} to solve the electronic and mass coupling between normal vibrational modes, leading to local modes that are free from any mode–mode coupling. A unique set of $3N - L$ (N = number of atoms; L = number of translations and rotations) local modes was determined for each complex, which could be connected to the normal modes in a one-to-one fashion via an adiabatic connection scheme.⁸²

The local stretching force constant (k^a) obtained from the corresponding local mode provides a direct measure of the intrinsic strength of a bond.⁸⁵ As pursued in our previous investigation on the halogen bonds strength,⁷⁶ the analysis of k^a was simplified by converting local stretching force constants into bond strength orders (BSOs) n . According to the generalized Badger rule,⁸⁶ BSO values are related to k^a via a power relationship (eq 1):

$$\text{BSO}_n = a(k^a)^b \quad (1)$$

Constants $a = 0.418$ and $b = 0.564$ were determined by assuming an n value of 1 for the FF bond in F_2 , $n = 0.5$ for the $3c-4e$ FF bond in $[\text{F}\cdots\text{F}\cdots\text{F}]^-$, and assuming an n value of zero for $k^a = 0$.

Binding energies were calculated with and without counterpoise (CP) correction⁸⁷ for the analysis of the basis set superposition error (BSSE). It is often observed that the CP correction does not necessarily lead to results closer to the complete basis set limit.⁸⁸ This is due to a fortuitous error cancellation present in uncorrected values.⁸⁹ Therefore, we decided to test whether CP-corrected or uncorrected interaction energies were closer to the values obtained with a larger basis set. For this purpose, the CP-corrected and uncorrected interaction energies of 12 complexes were calculated with domain-based local pair natural orbital DLPNO-CCSD(T) approximation^{90,91} utilizing both the aug-cc-pVTZ basis set and the more saturated aug-cc-pVSZ^{79,92} basis set. It turned out that the CP-uncorrected DLPNO-CCSD(T)/aug-cc-pVTZ values are on the average closer to CP-corrected and uncorrected DLPNO-CCSD(T)/aug-cc-pVSZ values (Supporting Information). Because of this, no attempt was made to include CP corrections to gradient or Hessian calculations.

Local properties of the electron density $\rho(\mathbf{r})$ and energy density distribution $H(\mathbf{r})$ obtained from CCSD(T) response densities were used to characterize the nature of the interactions. According to the Cremer–Kraka criteria for covalent bonding, a negative (stabilizing) energy density H_b at the bond critical point \mathbf{r}_b indicates predominant covalent

Table 1. Summary of Energetic, Geometric, and Vibrational Data for Complexes 1–32^a

complexes (sym)	$r(\text{XY})$	ΔE	ΔE	CP	$\rho_b(\text{YX})$	$H_b(\text{XY})$	CT	$\Delta E(\text{del})1$ WX ← Y	$\Delta E(\text{del})2$ X → YZ	$\Delta n(\text{WX})$ %	$\Delta n(\text{YZ})$ %	$k^2(\text{XY})$	$n(\text{XY})$	type
1	(Cl ₂) ₂ (C _{2h})	3.351	1.17	0.86	0.051	0.011	0.000	0.7	0.7	0	0	0.032	0.060	XB-I
2	(FCl) ₂ (C _{2h})	3.268	1.02	0.72	0.061	0.011	0.000	1.3	1.3	0	0	0.027	0.054	XB-I
3	(FBF ₂) ₂ (C _{2h})	3.195	1.65	1.26	0.110	0.002	0.000	5.0	5.0	-1	-1	0.046	0.073	XB-I
4	(Cl ₂) ₂ (C ₁)	3.330	1.56	1.20	0.054	0.012	-0.009	2.0	0.0	-1	0	0.043	0.071	XB-II
5	(FCl) ₂ (C ₂)	3.156	1.50	1.15	0.075	0.013	-0.017	4.5	0.2	-1	0	0.054	0.080	XB-II
6	(FBF ₂) ₂ (C ₂)	3.162	2.47	2.07	0.118	0.002	-0.046	12.5	0.7	-4	0	0.085	0.104	XB-II
7	(FSH) ₂ (C ₂)	2.748	4.44	3.61	0.229	-0.029	0.000	14.0	14.0	-12	-12	0.097	0.112	ChB-I
8	(FSH) ₂ (C ₁)	2.715	4.67	3.81	0.246	-0.035	0.000	15.8	15.8	-14	-14	0.095	0.111	ChB-I
9	(OH ₂ S) ₂ (C _{2h})	3.215	2.31	1.62	0.096	0.003	0.000	2.0	2.0	1	1	0.084	0.103	ChB-I
10	FHS...SHF (C ₁)	2.734	6.12	5.22	0.272	-0.049	-0.087	37.8	9.2	-14	-15	0.087	0.105	ChB-I
11	FHS...OFH (C ₁)	2.735	3.62	3.00	0.116	0.013	-0.016	6.4	0.8	-5	-1	0.104	0.116	ChB-II
12	FHS...OH ₂ (C ₁)	2.659	5.69	6.24	0.138	0.010	-0.028	9.4	0.1	-7	0	0.152	0.144	ChB-II
13	FHS...SH ₂ (C ₁)	3.065	4.53	4.00	0.123	0.000	-0.049	12.0	0.1	-9	0	0.107	0.118	ChB-II
14	FHS...SF ₂ (C ₁)	2.840	4.18	3.30	0.202	-0.019	-0.089	22.3	1.0	-12	0	0.077	0.098	ChB-II
15	(FH ₂ P) ₂ (C _{2h})	2.628	6.41	4.94	0.325	-0.087	0.000	28.2	28.2	-17	-17	0.143	0.139	PnB-I
16	(FH ₂ N) ₂ (C _{2h})	2.680	4.17	3.73	0.093	0.015	0.000	2.2	2.2	-1	-1	0.126	0.130	PnB-I
17	FH ₂ As...PH ₂ F (C ₁)	2.888	5.01	3.93	0.214	-0.037	-0.029	20.8	10.6	-14	-6	0.122	0.127	PnB-I
18	FH ₂ P...NH ₂ F (C ₁)	2.610	5.92	4.95	0.189	-0.017	-0.047	15.2	2.7	-19	0	0.120	0.126	PnB-II
19	FH ₂ P...PH ₃ (C ₁)	3.162	4.01	3.32	0.116	-0.005	-0.033	9.7	2.5	-17	1	0.079	0.100	PnB-II
20	FH ₂ P...NH ₃ (C ₂)	2.663	6.81	6.10	0.171	-0.012	-0.057	15.2	0.9	-21	0	0.144	0.140	PnB-II
21	FHS...PH ₂ F (C ₁)	2.493	6.10	4.84	0.408	-0.118	-0.103	47.3	24.2	-37	-17	0.103	0.116	PnB/ChB-I
22	FHS...PH ₂ F (C ₁)	2.578	8.21	7.03	0.392	-0.113	-0.150	63.7	17.6	-26	-13	0.217	0.176	PnB/ChB-I
23	FHS...AsH ₂ F (C ₁)	2.871	4.20	3.35	0.205	-0.027	-0.016	14.7	13.4	-10	-7	0.104	0.116	PnB/ChB-I
24	FH ₂ P...SH ₂ O (C ₁)	3.035	3.70	2.74	0.140	-0.010	-0.017	6.9	4.5	-13	1	0.087	0.105	PnB/ChB-I
25	FH ₂ P...SHF (C ₁)	3.186	3.30	2.56	0.102	-0.001	-0.039	9.0	0.2	-16	-3	0.075	0.097	PnB-II
26	FHS...PH ₂ F (C ₂)	2.841	4.66	3.89	0.211	-0.025	-0.088	22.3	0.5	-17	-11	0.080	0.100	ChB-II
27	FHS...PF ₂ H (C ₁)	2.624	4.92	3.79	0.318	-0.066	-0.135	40.9	2.9	-35	2	0.043	0.071	ChB-II
28	FHS...PH ₃ (C ₁)	2.946	4.87	4.29	0.168	-0.013	-0.062	16.6	0.1	-14	1	0.094	0.110	ChB-II
29	FH ₂ P...SH ₃ (C ₁)	2.104	3.68	3.08	0.088	0.001	-0.034	7.4	0.1	-16	0	0.087	0.105	PnB-II
30	FH ₂ P...SF ₂ (C ₁)	3.075	3.30	2.33	0.134	-0.008	-0.090	13.3	0.3	-16	0	0.082	0.102	PnB-II
31	FPH ₃ ...Cl ₂ (C ₁)	3.269	2.53	1.87	0.068	0.007	-0.035	4.2	0.1	-14	0	0.058	0.084	PnB-II
32	Cl ₂ ...PH ₂ F (C ₁)	3.221	2.38	1.93	0.098	0.007	-0.017	5.3	0.4	-12	-7	0.053	0.080	XB-II

^aComputed at CCSD(T)/aug-cc-pVTZ. Bond distance $r(\text{XY})$ in Å, binding energy ΔE and counterpoise (CP) corrected ΔE in kcal/mol. Density at XY critical point ρ_b in e/Å³, energy density at XY critical point H_b in hartree/Å³. NPA charge transfer in e, NBO delocalization energies computed with ω B97XD/aug-cc-pVTZ referent to lp(Y) → $\sigma^*(\text{WX})$ ($\Delta E(\text{del})1$) and lp(X) → $\sigma^*(\text{YZ})$ ($\Delta E(\text{del})2$) in kcal/mol, percent shifts in the BSO n values of WX and YZ (Δn (%)), $\text{YX } k^2$ in mdyÅ and BSO n values, noncovalent interaction type (see text).

character, whereas a positive (destabilizing) energy density indicates the formation of an electrostatic or dispersive interaction.^{93–95}

The possibility of electrostatic attraction between the unperturbed monomers was accessed by investigating the location and magnitude of the extreme values of the electrostatic potential $V(r)$ mapped onto the 0.001 e/bohr³ electron density surface of the monomers. The maximum $V(r)$ associated with the σ -hole region (V_{\max}) and the minimum (V_{\min}) associated with the lp(A) region provide an approximated measure for electrostatic attraction.^{96,97}

Covalent contributions to the intermolecular interactions were assessed via the analysis of the natural bond orbital (NBO) delocalization energies ($\Delta E(\text{del})$) associated with both lp(Y) $\rightarrow \sigma^*(\text{WX})$ and lp(X) $\rightarrow \sigma^*(\text{YZ})$ charge transfer mechanisms. The magnitude of $\Delta E(\text{del})$ was determined by second-order perturbation theory.⁹⁸ Due to the nonexistence of CCSD(T) orbitals, $\Delta E(\text{del})$ was calculated with $\omega\text{B97XD}/\text{aug-cc-pVTZ}$.^{99,100} Recently, Stone¹⁰¹ asserted that the NBO analysis overestimates charge transfer contribution to intermolecular interaction energies due to an inherent BSSE contamination, originated from the orthogonalization procedure adopted by the NBO analysis. Therefore, in this work, $\Delta E(\text{del})$ was only used for a qualitative analysis of lp(Y) $\rightarrow \sigma^*(\text{WX})$ and lp(X) $\rightarrow \sigma^*(\text{YZ})$ charge transfer mechanisms. No quantitative comparison between $\Delta E(\text{del})$ and ΔE or any other property was made. The $\Delta E(\text{del})$ analysis was complemented by the evaluation of the weakening of the WX and YZ bonds due to the partial occupation of $\sigma^*(\text{WX})$ and $\sigma^*(\text{YZ})$. This can be associated with the shift in the BSO values of the WX and YZ bonds, calculated according to eq 2:

$$\Delta n(\text{WX}) (\%) = \frac{n(\text{WX})_{\text{monomer}} - n(\text{WX})_{\text{dimer}}}{n(\text{WX})_{\text{monomer}} \times 100} \quad (2)$$

Deviations between trends in $\Delta E(\text{del})$ and $\Delta n(\text{WX}) (\%)$ indicate that contributions from other CT mechanisms or lone pair repulsion also influence the shifts in the strength of the WX and YZ bonds upon complex formation. The inspection of the CCSD(T) electron difference density distribution $\Delta\rho(\mathbf{r}) = \rho(\text{complex},\mathbf{r}) - \rho(\text{monomer1},\mathbf{r}) - \rho(\text{monomer2},\mathbf{r})$, determined for an electron density distribution of 0.001 e/bohr³ was also used to distinguish between electrostatic and covalent interactions. An accumulation of electron density in the XY bonding region indicates covalent character.

All local mode calculations were performed with COLOGNE2016.¹⁰² The CCSD(T) energy, energy gradient, and Hessian were calculated with CFOUR.¹⁰³ For the NBO analysis, NBO 6⁹⁸ was used, whereas the electron (energy) density distribution was investigated with the program AIMAll.¹⁰⁴ Correlated electron and energy density distributions were analyzed with the programs Molden2AIM, and MOLBO of Zou and co-workers.¹⁰⁵ The CCSD(T) electrostatic potential $V(r)$ were calculated with Multiwfn.¹⁰⁶

3. RESULTS AND DISCUSSION

Table 1 lists the noncovalent bond distances $r(\text{XY})$, the counterpoise corrected binding energies ΔE , the electron density ρ_b and the energy density H_b at the density critical point associated with the corresponding intermolecular interaction. The CT derived from the natural population analysis (NPA) atomic charges, the delocalization energy associated with the lp(Y) $\rightarrow \sigma^*(\text{WX})$ ($\Delta E(\text{del}1)$) and lp(X)

$\rightarrow \sigma^*(\text{YZ})$ ($\Delta E(\text{del}2)$) CT mechanisms, the percentage shift in the BSO n values ($\Delta n (\%)$) of W–X and Y–Z bonds upon the complex formation (eq 2), the local stretching force constant $k^a(\text{XY})$ and the BSO $n(\text{XY})$ associate with the noncovalent bond are also reported. The last column of Table 1 shows the type of the noncovalent interaction of each complex, classified according to the complex conformation as type I or II, and as XB, ChB, or PnB according to the stronger electron acceptor. In other words, if the largest $\Delta E(\text{del})$ value involves a $\sigma^*(\text{WX})$ where X is a halogen, the interaction is classified as a XB; likewise, if X is a chalcogen or a pnictogen the interaction is termed ChB or PnB.

Monomer properties are listed in Table 2, which includes the $r(\text{WX})$, $k^a(\text{WX})$, and $n(\text{WX})$ values, the vertical ionization

Table 2. Geometry, Vibrational Data, And Values of the Electrostatic Potential for the Monomers^a

	monomer	$r(\text{WX})$	$k^a(\text{WX})$	$n(\text{WX})$	IP	$V_{\max}(\text{X})$	$V_{\min}(\text{X})$
33	Cl ₂	2.019	3.025	0.780	11.5	1.10	−0.13
34	FCl	1.646	4.326	0.954	12.7	1.75	−0.01
35	FBr	1.770	4.019	0.915	11.9	2.12	0.01
36	FHS	1.626	4.569	0.984	10.4	1.75	−0.43
37	FHSe	1.765	3.998	0.913	9.9	2.02	−0.37
38	OH ₂ S	1.504	7.163	1.268	10.2	1.77	0.02
39	H ₂ S	1.342	4.249	0.945	10.4		−0.71
40	F ₂ S	1.607	4.729	1.003	10.3	1.61	−0.20
41	H ₂ O	0.962	8.260	1.375	12.7		−1.40
42	OHF	1.442	4.280	0.949	12.9		−0.72
43	AsH ₂ F	1.761	3.991	0.912	8.7	1.83	−0.19
44	PH ₂ F	1.577	5.791	1.125	10.1	1.59	−0.48
45	NH ₂ F	1.433	4.138	0.931	11.6	1.40	−1.21
46	PF ₂ H	1.427	3.150	0.798	11.0	0.88	−0.26
47	PH ₃	1.420	3.331	0.823	10.5	0.53	−0.68
48	NH ₃	1.015	6.798	1.232	10.9		−1.62

^aDistances $r(\text{WX})$ in Å, WX local stretching force constants in mdyn/Å, and bond strength order $n(\text{WX})$. Vertical ionization potential, maximum electrostatic potential at the σ -hole of X, and minimum electrostatic potential at the lp(X) in eV. All values were calculated with CCSD(T)/aug-cc-pVTZ.

potential (IP) and the extreme values of the electrostatic potential in the lone pair region (V_{\min}) and in σ -hole region (V_{\max}) of the atom X. Figure 3 shows the bond strength ordering of all noncovalent interactions investigated in this

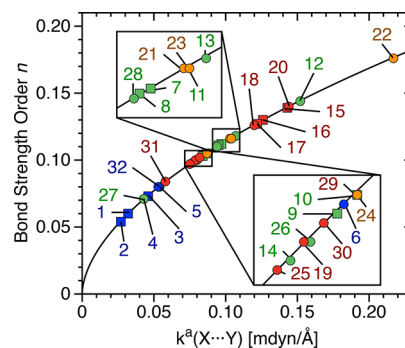


Figure 3. Power relationship between the relative bond strength order (BSO) n and the local stretching force constants k^a of complexes 1–32. XB in blue, ChB in green, PnB in red, and the mixed ChB/PnB in orange. Type I complexes are denoted by circles, and type II, by squares. Calculate at CCSD(T)/aug-cc-pVTZ level.

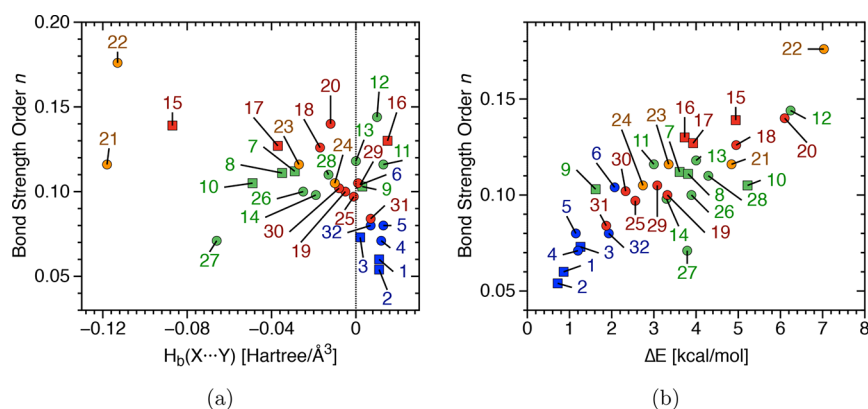


Figure 4. Comparison of the relative bond strength order (BSO) n with (a) the energy density at the bond critical point H_b of the ChBs of complexes 1–32 and with (b) binding energies (ΔE) for complexes 1–32. XB are shown in blue, ChB in green, PnB in red and the ChB/PnB in orange. Type I complexes are denoted by circles and type II by squares. Calculate at CCSD(T)/aug-cc-pVTZ level.

work, ranging from BSO $n = 0.054$ (complex 2) to 0.176 (complex 22). Compared to the BSO values obtained in our previous studies on XB,^{22,24,76} ChB,²³ and PnB,^{54,55} the interactions considered in the present study can be classified as weak (BSO < 0.2 and $\Delta E < 10$ kcal/mol). According to the Cremer–Kraka criteria, about half of these complexes have a dominant electrostatic character with $H_b \gtrsim 0.0$ and the others have partial covalent contributions $H_b < 0$.

Comparison of BSO n Values and Other Properties. A comparison of the BSO n values and H_b is given in Figure 4a. It is commonly found that as noncovalent interactions become stronger, they tend to have a higher covalent character.^{22,23,76} However, for the relatively weak complexes considered in the present study, electrostatic interactions are able to surpass interactions with covalent character. This is in particular observed for interactions involving O and N atoms, which are not as polarizable as P, S, As, or Se but have a more negative electrostatic potential in the lp(X) region.

There is a scattered correlation between BSO n values and ΔE (Figure 4b). The latter is a cumulative quantity that measures the energy required for the dissociation of the complexes into monomers, which includes besides the atom-to-atom bond strength, the energy required for the reorganization of the electron density and geometry of the monomers, and the fraction of any secondary intermonomers interactions that does not contribute to the atom-to-atom bond strength. Because of these reasons ΔE does not reflect the intrinsic strength of the noncovalent interactions.^{76,107,108}

Bonding Mechanism of Type I and II Complexes. In the present work we used the following protocol to analyze the strength and nature of the noncovalent interactions. First, the energy density is used to distinguish between interactions of dominant electrostatic and covalent character. Second, the strength of electrostatic interactions is rationalized on the basis of the analysis of the electrostatic potentials of the unperturbed monomers. Third, electrostatic interactions involving a weak electrostatic potential are considered to be dispersive and their strength is rationalized on the basis of polarizabilities. The fourth and last step is the analysis of covalent contributions on the basis of charge transfer involving specific orbitals.

On the basis of the protocol adopted, we can distinguish noncovalent interactions stabilized by electrostatic, covalent, and dispersive contributions in the following way: The electrostatic part refers to the attraction between the negative electrostatic potential in the lone pair region of atom Y and the

positive electrostatic potential formed at the σ -hole (region of depleted electron density formed collinear to a σ -bond) at the atom X (of the unperturbed monomers). Type II complexes tend to form stronger electrostatic attractions due to the collinear orientation between the negative electrostatic potential at the lp(Y) and the positive potential at the σ -hole of the WX bond, whereas the skewed orientation of type I complexes leads to a less effective alignment between the lp and the σ -hole electrostatic potential of the monomers. Electro-negative substituents withdraw charge from X and Y strengthening the positive potential at the σ -hole, but weakening the negative potential at the lone pair region.

Covalent contributions are rationalized in terms of the CT mechanism described in the orbital interaction diagram depicted in Figure 5. In type II complexes the covalent

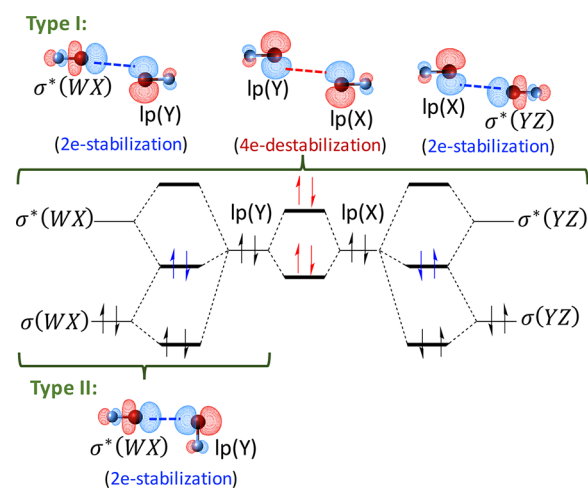


Figure 5. Orbital interaction diagram for type I and type II complexes, showing lp \rightarrow σ^* (2e stabilization) and lp–lp (4e destabilization) charge transfer mechanisms for complexes 2 and 5.

contribution involves the charge transfer from the lp(Y) to the $\sigma^*(WX)$ orbital, leading to 2e-delocalization and 2e-stabilization. A similar situation is also observed for type I complexes. However, the monomers in type I complexes adopt a skewed conformation allowing in addition the CT from the lp(X) to the $\sigma^*(YZ)$ orbital, leading not only to an extra 2e-stabilization but also to a 4e-destabilization due to lp(X)–lp(Y) repulsion. The 2e-stabilization and 4e-destabilization are proportional to

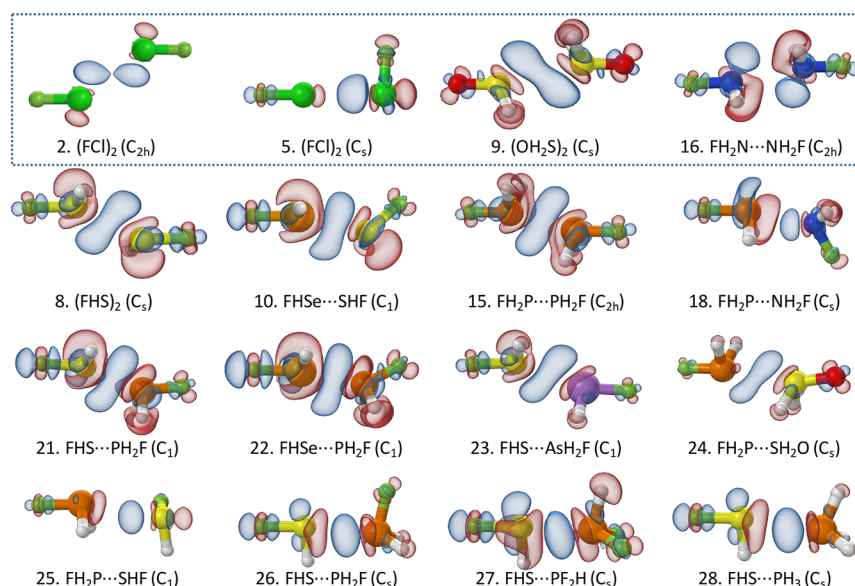


Figure 6. Electron difference density distributions $\Delta\rho(r)$ given for selected complexes. $\Delta\rho(r)$ is plotted for an electron density surface of 0.0004 au for the complexes in the rectangle (first row) and 0.001 au for the others. Blue regions indicate an increase in the electron density; red regions, a density decrease relative to the superimposed density of the monomers. Calculate at CCSD(T)/aug-cc-pVTZ level.

the magnitude of the orbital overlap and inversely proportional to the orbital energy gap ($\Delta\epsilon$) between the molecular orbitals involved. Although only one CT mechanism is present in type II complexes, the $\text{lp}(Y)-\sigma^*(WX)$ head-on overlap is more effective compared to the skewed overlap in type I complexes, and more importantly, the $\text{lp}(X)-\text{lp}(Y)$ repulsion in type II complexes is minimized due to the smaller overlap.

The CT can be magnified by decreasing the $\sigma^*(WX)$ and the $\sigma^*(YZ)$ orbital energies or by increasing the $\text{lp}(X)$ and $\text{lp}(Y)$ orbital energies. A more electronegative W substituent lowers the energy of the $\sigma(WX)$ and $\sigma^*(WX)$ orbitals, thus decreasing the energy gap between $\text{lp}(Y)$ and $\sigma^*(WX)$. The $\text{lp}(Y)-\sigma(WX)$ orbital overlap is also improved by an electronegative W substituent, which reduces the X coefficient of the $\sigma(WX)$ orbital. Due to orbital orthogonality, this in turn leads to a larger coefficient of $\sigma^*(WX)$ orbital, thus increasing the $\text{lp}(Y)-\sigma^*(WX)$ orbital overlap. An electronegative W atom also contracts the density at the X atom affecting the $\text{lp}(X)$ orbital in two different ways (i) for atoms of the second period of the PT, the $\text{lp}(X)$ orbitals becomes too compact decreasing $\text{lp}(X)-\sigma^*(YZ)$ orbital overlap (ii) for atoms of the third or higher periods of the PT, the $\text{lp}(X)$ becomes less diffuse, leading to improved $\text{lp}(X)-\sigma^*(YZ)$ orbital overlap.²³

Dispersive contributions play a dominant role only for complexes with minimal electrostatic and covalent contributions. In these cases the strength of the interaction can be rationalized on the basis of the polarizability of the monomers involved.

The different bonding mechanisms of type I and type II complexes are expected to result in different electronic structure changes upon complexation. This is demonstrated by the $\Delta\rho(r)$ plots shown in Figure 6. Type II complexes (e.g., complexes 5, 18, 25, 26, 27, and 28 in Figure 6) are easily identify by a round shaped increase in the electron density in the intermonomer region (in blue), whereas type I complexes have a more stretched region of increased electron density (e.g., complexes 2, 8, 9, 10, 15, 21, 22, 23, and 24 in Figure 6). Therefore, rather than relying solely on geometric parameters we will make use of $\Delta\rho(r)$ and the properties described in

Table 2 to distinguish between type I or type II complexes in the next sections.

Halogen...Halogen Interactions (Complexes 1–6).

Complexes 1–6 are only of electrostatic or dispersive nature. The high electronegativity of the halogen atoms results in X and Y lone pairs, which are too low in energy compared to the $\sigma^*(WX)$ and $\sigma^*(YZ)$ orbitals to lead to an effective CT (there is a large $\Delta\epsilon(2e)$ energy gap). Therefore, small $\Delta E(\text{del})$ and Δn (%) values are observed. The electrostatic potential at the lone pair (π) region of the halogen Y is close to zero ($V_{\text{min}} = -0.13$ eV for Cl_2 , -0.01 eV for FCl, and 0.01 eV for FBr), resulting in weak electrostatic attraction with the V_{max} at the σ -hole of X atoms. The skewed conformation of XB-I complexes 1–3 leads to an even poorer electrostatic attraction between the extreme electrostatic potentials in the lp and in the σ -hole regions.

The strength of complexes 1–3 can only be rationalized on the basis of the polarizability of the monomers, in particular of the X and Y atoms. For these complexes the BSO n increases in the series $(\text{FCl})_2$ (2) < $(\text{Cl}_2)_2$ (1) < $(\text{FBr})_2$ (3). The high polarizing power of the F substituents in 2 withdraws charge from Cl, decreasing its effective radius and, as a result, 2 has a Cl...Cl distance 0.083 Å shorter than that found in 1. However, due to the lower polarizability of FCl compared to Cl_2 , complex 2 forms a weaker interaction (BSO n : 0.060 (1), 0.054 (2)). In the case of $(\text{FBr})_2$ the higher polarizability of Br compared to that of Cl, leads to a stronger bond (BSO n : 0.073 (3)).

By adopting a conformation in which the positive potential at the σ -hole is collinear with the negative potential of the lone pairs, XB-II complexes (4–6) are able to form true XBs. The strength of the XB in these complexes increases in the order $(\text{Cl}_2)_2$ (4) < $(\text{FCl})_2$ (5) < $(\text{FBr})_2$ (6) and is determined by the magnitude of V_{max} at the σ -hole of X (Table 2). Although FBr has a slightly positive potential at the π region of Br suggesting a $\text{lp}(\text{Br})\cdots\sigma\text{-hole}(\text{Br})$ repulsive interaction, one has to consider that the strong V_{max} at the Br σ -hole polarizes the π density of the second Br. An inverse relationship between ΔE and the BSO n is found for complexes 4 and 5, indicating that secondary effects besides the $\text{Cl}\cdots\text{Cl}$ XB help to stabilize

complex **4**. This is evidenced by the inward tilted $\theta_2 = 88.5^\circ$ angle adopted by **4** compared to the outward angle $\theta_2 = 95.3^\circ$ of **5**.

Chalcogen...Chalcogen Interactions (Complexes 7–14). There are two minima of ChB-I type for (FHS)₂ complexes (**7**, **8**). One with C₂ symmetry where the H atoms are in a syn position (**7**), and the other with C_i symmetry, where the H atoms are anti to each other (**8**). Both complexes are twice as strong as the isoelectronic XB-I complex **2**, with YX distances of 2.748 Å for **7** and 2.715 Å for **8** compared to 3.268 for **2**. The shorter and stronger interaction of these complexes is due to the more effective charge transfer ($\Delta E(\text{del}) = 14.0$ (**7**), 15.8 (**8**), 1.3 (**2**) kcal/mol). Compared to Cl lone pairs, the lone pairs of S are higher in energy (IP: 12.7 kcal/mol for FCl and 10.4 kcal/mol for FHS), resulting in a smaller $\Delta\epsilon(2e)$ energy gap. The lp- σ^* overlap is also improved due the lower electronegativity of S compared to Cl (leading to a larger X coefficient in the $\sigma^*(\text{WX})$ orbital). Due to the large lp(S)- $\sigma^*(\text{SO})$ energy gap and the weak electrostatic attraction, (OH₂S)₂ (**9**) forms a weak ChB-I.

If one S atom in **8** is substituted by the more polarizable Se, the heterodimer **10** (FHSe...SHF) is formed. This complex has a distorted geometry ($\theta_1 = 162.8^\circ$ and $\theta_2 = 125.2^\circ$), favoring a stronger electrostatic attraction between the Se σ -hole and the lp(S) and the CT from lp(S) $\rightarrow \sigma^*(\text{SeF})$. However, partial ChB-I character is still maintained. This is evidenced from the $\Delta\rho(r)$ shown in Figure 6 by the stretched area of electron density increase (in blue), characteristic of type I complexes, and is confirmed by the sizable lp(Se) $\rightarrow \sigma^*(\text{SF})$ 2e-stabilization ($\Delta(\text{del})2 = 9.2$ kcal/mol) and by the weakening of both SF and SeF bonds by 14% and 15%, respectively (Table 1). It is noteworthy that the ΔE of **10** is 1.4 kcal/mol larger than that of complex **8**, but the BSO n of **10** is 0.105 compared to 0.111 in **8**, suggesting that the geometry of this complex is distorted, not only to maximize the Se...S interaction but also due to the electrostatic attraction between the positively charged Se and the negative charge at the F. This is also reflected by the opposite trends between $\Delta E(\text{del})$ and Δn (%) values (Table 1). Although $\Delta E(\text{del})1$ (referent to lp(S) $\rightarrow \sigma^*(\text{SeF})$ CT) is much larger than $\Delta E(\text{del})2$ (referent to lp(S) $\rightarrow \sigma^*(\text{SeF})$ CT), both SF and SeF bonds are weakened by about 15%.

In contrast, if S is substituted with the less polarizable O, only a ChB-II is formed (**11**). The OHF monomer has a lp(O) that is too low in energy (IP = 12.9 eV (OHF), 12.7 eV (OH₂) compared to 10.4 eV (FHS)), leading to a large $\Delta\epsilon(2e)$, and thereby to a small CT. The large negative potential at the lp(O) (V_{min} : -1.40 eV (OH₂) compared to -0.43 eV (FHS)) allows **12** to form an electrostatic interaction that is stronger than interactions with partial covalent character, such as the ones in complexes **8** and **10**.

When an F atom is substituted with a H in complex **8**, a stronger ChB (BSO n : 0.118 (**13**), 0.111 (**8**)) with lower covalent character, but improved electrostatic contribution, is formed (**13**). However, if a H atom is substituted by an F atom in **8**, a weaker interaction (BSO n : 0.098 (**14**), but with a higher covalent character than **13**, is formed. The extra F atom in **14** has a small impact on the lp(S) energy (IP: 10.3 eV for SF₂, 10.4 eV for SFH); however, due to the high electronegativity of F, the electron density at the S atom is contracted leading to a shorter interaction distance ($r(\text{SS}) = 2.840$ Å (**14**) compared to 3.065 Å (**13**)) and to a more effective lp(S)- $\sigma^*(\text{SF})$ overlap.

Similar effects are also present in XB and other ChB complexes.^{23,76}

Pnicogen...Pnicogen Interactions (Complexes 15–20). Complex **15** ((FH₂P)₂) forms a shorter, stronger, and more covalent interaction than the isoelectronic XB-I (**2**) and ChB-I (**8**) complexes. P is less electronegative than S or Cl, thereby the lp(P) orbital is higher in energy, resulting in a smaller $\Delta\epsilon(2e)$ energy gap and a stronger CT. Surprisingly, the complex formed by substituting both P atoms by the N (**16**) is also stronger than complexes **2** and **8**. Different from **15**, complex **16** has a high $\Delta\epsilon(2e)$ energy gap and no significant covalent contribution; however, the lp(N) can form an electrostatic attraction with the positively charged H atoms at the opposite NH₂F monomers. This electrostatic attraction is favored by the lp(N)-lp(N) repulsion, which pushes the electron density from the inter nitrogens region into the direction of the hydrogens (Figure 6).

Similar to the case for the chalcogens, substituting a P atom in **15** with the larger and more polarizable As yields a PnB-I complex (**17**) weaker than **15** (BSO n : 0.127 (**17**), 0.139 (**15**)). If a P atom is replaced with a N atom the PnB-II complex **18** is formed. This complex is weaker than both **15** and **16** (BSO n = 0.126 (**18**), 0.130 (**16**), 0.139 (**15**)).

A PnB-II complex with a BSO n comparable to that of the strongest PnB-I (complex **15**) is realized for FH₂P...NH₃ (**20**). The CT in **20** is similar to that in **18** (Table 1); however, due to the absence of an F substituent NH₃ has a lower electrostatic potential at the N than NH₂F ($V_{\text{min}} = -1.21$ eV (NH₂F), -1.61 eV (NH₃)). This results in a stronger electrostatic attraction with the σ -hole of FH₂P. Noteworthy is that although **20** and **15** have BSO n values of 0.14, complex **20** has a ΔE 1.16 kcal/mol larger than that of **15**. The extra stabilization in **20** is easily understood by considering the orientation of the dipoles moment of the monomers, which have opposite directions in **15** but the same direction in **20**.

Interactions Involving Atoms of Different Groups (Complexes 21–32). From the investigation of XB-I, ChB-I, and PnB-I complexes it becomes evident that an interaction involving atoms of different groups of the periodic table (PT), which is capable of retaining a type I character is more likely a chalcogen-pnicogen combination. This is confirmed for complexes **21–24**, where two CT mechanisms, one characteristic of a ChB and one characteristic of a PnB, are present. Therefore, these complexes were classified as a PnB/ChB-I type in this work. These complexes also have a $\Delta\rho(r)$ that resembles those of the other type I complexes (Figure 6).

The combination of the monomers involved in the strongest ChB-I (**7**) and PnB-I (**15**) complexes leads to FHS...PH₂F. This complex has three different minimum-energy conformations: one forming a PnB/ChB-I complex (**21**), one forming a PnB-II complex **25**, and the other forming a ChB-II complex (**26**). The presence of both a charge transfer from lp(S) to $\sigma^*(\text{PF})$ and also from lp(P) to $\sigma^*(\text{SF})$ in **21** leads to an extra stabilization and to a stronger interaction compared to **25** and **26** (BSO n = 0.116 (**21**), 0.097 (**25**), 0.100 (**26**)), but weaker compared to the PnB-I homodimer **15** (BSO n = 0.139).

A complex with partial PnB/ChB-I character and a stronger noncovalent interaction than **15** is obtained by substituting S by Se in **21** (complex **22**). Similar to **10**, complex **22** has a distorted geometry favoring lp(P) $\rightarrow \sigma^*(\text{SeF})$ CT and lp(Se)- σ -hole electrostatic attraction ($\Delta(\text{del})1 = 63.7$ kcal/mol (**22**) compared to 47.3 kcal/mol (**21**)) in detriment of lp(Se) $\rightarrow \sigma^*(\text{PFH}_2)$ CT ($\Delta(\text{del})2 = 17.6$ kcal/mol (**22**)).

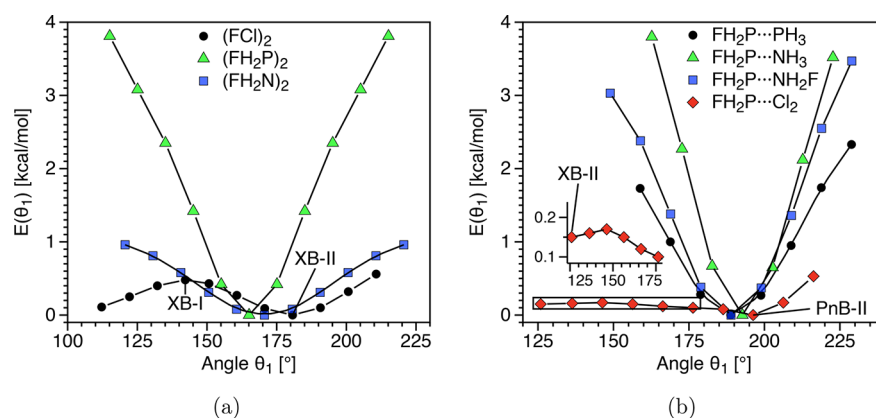


Figure 7. Relationship between the potential energy relative to the minimum energy point and θ_1 for (a) homodimers (b) PnB heterodimers. Black lines are used just to connect points.

compared to 24.2 kcal/mol (**21**). Because of the substantial stabilization from both CT mechanisms and due to the characteristic $\Delta\rho(r)$ of type I complexes (Figure 6), complex **22** is still of type I. If the P atom in **21** is replaced by a As, a complex of similar strength to **21** and with an equivalent admixture of PnB and ChB character is formed ($\Delta E(\text{del}1) \approx \Delta E(\text{del}2)$) (**23**). The higher polarizability of As in **23** results in a more diffuse lp(As), leading to a longer interaction distance with a less effective lp(As)– $\sigma^*(\text{SF})$ overlap, thus to a smaller CT. This is counterbalanced by the higher electrostatic potential at the As σ -hole, increasing the electrostatic contribution.

The combination of FPH₂ and SH₂O also leads to a type I complex (**23**). This complex has an intermediate strength between the homodimers (OH₂S)₂ (**9**) and (FH₂P)₂ (**15**). Similar to what was observed for chalcogen...chalcogen and pnictogen...pnictogen complexes, substituting a F atom with a H or vice versa only type-II complexes are formed (**27–30**).

Sensitivity to Angular Distortion. To measure the angular distortion sensitivity for a set of seven complexes, the θ_1 angle was distorted from its fully optimized geometry in increments of 10°. At each step all geometric parameters but θ_1 were reoptimized. Figure 7 shows how the energy relative to the undistorted geometry varies as a function of θ_1 for three homodimers (Figure 7a) and four heterodimers (Figure 7b).

Type XB-I complexes (**1–3**) are first-order transition states. The imaginary frequencies of these complexes are of 12 (**1**), 25 (**2**), and 30 (**3**) cm⁻¹ and can be associated with the W–X–Y bending mode that leads to the type XB-II complexes **4**, **5**, and **6**, respectively. The bending potential of (FCl)₂ (complex **2**) shown in Figure 7 reveals that there is a small difference between the high-energy XB-I and the minimum-energy XB-II conformations (0.48 kcal/mol for (FCl)₂ 0.39 kcal/mol for (Cl₂)₂, and 0.83 kcal/mol for (FBr)₂), which could easily be overcome by crystal packing forces. This observation is in line with experimental studies on the halogen...halogen interactions in hexahalogenated benzenes, suggesting that Cl...Cl and Br...Br interactions are weak and nondirectional and can be easily deformed leading to a conformation that does not correspond strictly to type I or type II conformation.⁵³

Other type I homodimers held together by stronger interactions such as (FNH₂)₂ and (FPH₂)₂ are minima in the potential energy surface. In these cases, the angular sensitivity increases with the increased strength and covalent character of the interaction. No type II minimum was found for these

complexes. The angular sensitivity in type II heterodimers also increases with the strength of the interaction following the order FH₂P...Cl₂ < FH₂P...PH₃ < FH₂P...NH₂F < FH₂P...NH₃ (Figure 7b).

Although only a XB-II and a PnB-II minimum and no XB/PnB type I minimum-energy point were identified by bending Cl₂...PFH₂, the barrier separating the PnB-II complex **31** from the XB-II complex **32** is just 0.15 kcal/mol, suggesting that a dispersive force (similar to the ones found for complexes **1–3**) lowers the barrier separating these two types of interactions.

4. CONCLUSIONS AND OUTLOOK

In the present work, we compared the nature, the intrinsic strength, and the binding energies of a series of weak noncovalent interactions involving pnictogen, chalcogens, and halogens atoms using highly accurate CCSD(T)/aug-cc-pVTZ geometries, vibrational frequencies, NPA atomic charges, energy and electron densities, and electrostatic potentials. By generalizing the description of type I and II interactions commonly employed for halogen...halogen complexes and including suitable molecular orbital diagrams, we obtained the following conclusions:

1. Noncovalent interactions involving chalcogens, pnictogens, and halogens can be described by a similar bonding mechanism, which only depends on the conformation adopted by the complex. Type I complexes adopt a skewed conformation allowing two different CT mechanisms (from the lp(Y) to the $\sigma^*(\text{WX})$ orbital and from the lp(X) to the $\sigma^*(\text{YZ})$ orbital), whereas type II complexes adopt a conformation where lp(Y) is collinear to $\sigma^*(\text{WX})$, maximizing the charge transfer from the lp(Y) to the $\sigma^*(\text{WX})$ orbital.
2. Instead of relying solely on geometric parameters, we used for the first time in addition, electron difference densities, delocalization energies, and the shift in the bond strength order of the WX and YZ bonds to distinguish between type I and type II complexes. In this connection, type I complexes are easily distinguished by the stretched area of electron density increase in the intermonomer region, when compared to type II complexes.
3. Pnictogens can form stronger type I homodimers than chalcogens or halogens. The lower electronegativity of P compared to that of S or Cl leads to a smaller $\Delta\epsilon(2e)$ energy gap, granting partial covalent character to the P...

P interactions. The higher electronegativity of halogens results in XB-I complexes of dispersive nature, which are first-order transition states.

- Heterodimers can also form type I complexes as long as the $\text{lp}(Y)-\sigma^*(\text{WX})$ and the $\text{lp}(X)-\sigma^*(\text{YZ})$ orbital overlaps and the orbital energy gaps are small. $\text{FHS}\cdots\text{PH}_2\text{F}$ is an example of a stable type I complex involving two CT mechanisms, one characteristic of a PnB and the other of a ChB. This PnB/ChB-I complex is stronger than the ChB-II or PnB-II complexes formed by the same monomers.
- There is a scattered correlation between the binding energies and the intrinsic bond strength given by the k^3 or BSO n values for all complexes investigated in this work. This scattering occurs when secondary contributions, not accounted for by the atom–atom interaction, are involved in the stabilization of the complex. The comparison of BSO and ΔE trends are useful to identify the significance of such contributions.

Clark, Politzer, and Murray^{96,97,109} recently suggested the analysis of the unperturbed electrostatic potentials of the monomers mapped onto a van der Waals surface as a practical approximation to predict the geometry and even the strength of noncovalent interactions that are not affected by polarization. However, a caveat is appropriate. Polarization can play a decisive role even for weak interactions (e.g., $\Delta E < 10$ kcal/mol). In these cases, orbital interaction diagrams (although based on model quantities rather than physical observables) provide the most insightful and intuitive way to describe the mechanism of these noncovalent interactions. When a specific charge transfer mechanism is singled out, a simple orbital interaction diagram can be used to rationalize the covalent contributions of the interactions involving halogens, chalcogens, and pnictogens of both type I and II conformations.

■ ASSOCIATED CONTENT

Supporting Information

The Supporting Information is available free of charge on the ACS Publications website at DOI: 10.1021/acs.jpca.7b10196.

CP-corrected and uncorrected interaction energies of 12 complexes calculated with DLPNO-CCSD(T)/aug-cc-pVTZ, and DLPNO-CCSD(T)/aug-cc-pV5Z, molecular electrostatic potential of all monomers, selected molecular orbitals of the monomers, and complex geometries (PDF)

■ AUTHOR INFORMATION

Corresponding Author

*E. Kraka. E-mail: ekraka@smu.edu.

ORCID

Elfi Kraka: 0000-0002-9658-5626

Notes

The authors declare no competing financial interest.

■ ACKNOWLEDGMENTS

This work was financially supported by the National Science Foundation grants CHE 1152357 and CHE 1464906. We thank SMU for providing computational resources. The authors acknowledge financial support by CAPES (Brazil; fellowship grant BEX 9534-13-0).

■ DEDICATION

Dedicated to the memory of Professor Dieter Cremer, whose pioneering work and insightful discussions on noncovalent interactions and vibrational spectroscopy were fundamental to this study.

■ REFERENCES

- Cavallo, G.; Metrangolo, P.; Milani, R.; Pilati, T.; Priimagi, A.; Resnati, G.; Terraneo, G. The halogen bond. *Chem. Rev.* **2016**, *116*, 2478–2601.
- Matta, C. F.; Castillo, N.; Boyd, R. J. Extended weak bonding interactions in DNA: π -stacking (base-base), base-backbone, and backbone-backbone interactions. *J. Phys. Chem. B* **2006**, *110*, 563–578.
- Sponer, J.; Riley, K. E.; Hobza, P. Nature and magnitude of aromatic stacking of nucleic acid bases. *Phys. Chem. Chem. Phys.* **2008**, *10*, 2595–2610.
- Bissanz, C.; Kuhn, B.; Stahl, M. A medicinal chemist's guide to molecular interactions. *J. Med. Chem.* **2010**, *53*, 5061–5084.
- Wilcken, R.; Zimmermann, M. O.; Lange, A.; Joerger, A. C.; Boeckler, F. M. Principles and applications of halogen bonding in medicinal chemistry and chemical biology. *J. Med. Chem.* **2013**, *56*, 1363–1388.
- Wheeler, S. E.; Seguin, T. J.; Guan, Y.; Doney, A. C. Noncovalent interactions in organocatalysis and the prospect of computational catalyst design. *Acc. Chem. Res.* **2016**, *49*, 1061–1069.
- Uyeda, C.; Jacobsen, E. N. Transition-state charge stabilization through multiple non-covalent interactions in the guanidinium-catalyzed enantioselective claisen rearrangement. *J. Am. Chem. Soc.* **2011**, *133*, 5062–5075.
- Yáñez, M.; Sanz, P.; Mó, O.; Alkorta, I.; Elguero, J. Beryllium bonds, do they exist? *J. Chem. Theory Comput.* **2009**, *5*, 2763–2771.
- Tama, R.; Mó, O.; Yáñez, M.; Montero-Campillo, M. M. Characterizing magnesium bonds: main features of a non-covalent interaction. *Theor. Chem. Acc.* **2017**, *136*, 36.
- Bauzá, A.; Frontera, A. Aerogen bonding interaction: A new supramolecular force? *Angew. Chem., Int. Ed.* **2015**, *54*, 7340–7343.
- Bauzá, A.; Mooibroek, T. J.; Frontera, A. Tetrel-bonding interaction: Rediscovered supramolecular force? *Angew. Chem., Int. Ed.* **2013**, *52*, 12317–12321.
- Del Bene, J. E.; Alkorta, I.; Elguero, J. In *Noncovalent forces*; Scheiner, S., Ed.; Springer International Publishing: Berlin, 2015; pp 191–263.
- Zhang, X.; Dai, H.; Zou, H. Y. W.; Cremer, D. B-H \cdots π interaction: A new type of nonclassical hydrogen bonding. *J. Am. Chem. Soc.* **2016**, *138*, 4334–4337.
- Stone, A. J. Are halogen bonded structures electrostatically driven? *J. Am. Chem. Soc.* **2013**, *135*, 7005–7009.
- Wang, C.; Guan, L.; Danovich, D.; Shaik, S.; Mo, Y. The origins of the directionality of noncovalent intermolecular interactions. *J. Comput. Chem.* **2016**, *37*, 34–45.
- Politzer, P.; Murray, J. S.; Clark, T. Halogen bonding: An electrostatically-driven highly directional noncovalent interaction. *Phys. Chem. Chem. Phys.* **2010**, *12*, 7748–7757.
- Esrifili, M. D.; Mohammadirad, N. An ab initio study on tunability of σ -hole interactions in XHS:PH₂Y and XH₂P:SHY complexes (X = F, Cl, Br; Y = H, OH, OCH₃, CH₃, C₂H₅, and NH₂). *J. Mol. Model.* **2015**, *21*, 176.
- Albrecht, L.; Boyd, R. J.; Mó, O.; Yáñez, M. Changing weak halogen bonds into strong ones through cooperativity with beryllium bonds. *J. Phys. Chem. A* **2014**, *118*, 4205–4213.
- Alkorta, I.; Elguero, J.; Mó, O.; Yáñez, M.; Del Bene, J. E. Using beryllium bonds to change halogen bonds from traditional to chlorine-shared to ion-pair bonds. *Phys. Chem. Chem. Phys.* **2015**, *17*, 2259–2267.
- Brea, O.; Mó, O.; Yáñez, M.; Alkorta, I.; Elguero, J. Creating σ -holes through the formation of beryllium bonds. *Chem. - Eur. J.* **2015**, *21*, 12676–12682.

- (21) M6, O.; Y6nez, M.; Alkorta, I.; Elguero, J. Modulating the strength of hydrogen bonds through beryllium bonds. *J. Chem. Theory Comput.* **2012**, *8*, 2293–2300.
- (22) Oliveira, V.; Kraka, E.; Cremer, D. Quantitative assessment of halogen bonding utilizing vibrational spectroscopy. *Inorg. Chem.* **2017**, *56*, 488–502.
- (23) Oliveira, V.; Cremer, D.; Kraka, E. The many facets of chalcogen bonding: Described by vibrational spectroscopy. *J. Phys. Chem. A* **2017**, *121*, 6845–6862.
- (24) Oliveira, V.; Cremer, D. Transition from metal-ligand bonding to halogen bonding involving a metal as halogen acceptor a study of Cu, Ag, Au, Pt, and Hg complexes. *Chem. Phys. Lett.* **2017**, *681*, 56–63.
- (25) Bai, M.; Thomas, S. P.; Kottokkaran, R.; Nayak, S. K.; Ramamurthy, P. C.; Guru Row, T. N. A donor-acceptor-donor structured organic conductor with S...S chalcogen bonding. *Cryst. Growth Des.* **2014**, *14*, 459–466.
- (26) Atzori, M.; Artizzu, F.; Sessini, E.; Marchio, L.; Loche, D.; Serpe, A.; Deplano, P.; Concas, G.; Pop, F.; Avarvari, N.; et al. Halogen-bonding in a new family of tris(haloanilato)metallate(iii) magnetic molecular building blocks. *Dalton Trans.* **2014**, *43*, 7006–7019.
- (27) Yamamoto, H. M.; Yamaura, J.-I.; Kato, R. Multicomponent molecular conductors with supramolecular assembly: Iodine-containing neutral molecules as building blocks. *J. Am. Chem. Soc.* **1998**, *120*, 5905–5913.
- (28) Virkki, M.; Tuominen, O.; Forni, A.; Saccone, M.; Metrangolo, P.; Resnati, G.; Kauranen, M.; Priimagi, A. Halogen bonding enhances nonlinear optical response in poled supramolecular polymers. *J. Mater. Chem. C* **2015**, *3*, 3003–3006.
- (29) Zhu, W.; Zheng, R.; Zhen, Y.; Yu, Z.; Dong, H.; Fu, H.; Shi, Q.; Hu, W. Rational design of charge-transfer interactions in halogen-bonded co-crystals toward versatile solid-state optoelectronics. *J. Am. Chem. Soc.* **2015**, *137*, 11038–11046.
- (30) Priimagi, A.; Cavallo, G.; Forni, A.; Gorynsztejn-Leben, M.; Kaivola, M.; Metrangolo, P.; Milani, R.; Shishido, A.; Pilati, T.; Resnati, G.; et al. Halogen bonding versus hydrogen bonding in driving self-assembly and performance of light-responsive supramolecular polymers. *Adv. Funct. Mater.* **2012**, *22*, 2572–2579.
- (31) Ho, P. C.; Szydowski, P.; Sinclair, J.; Elder, P. J. W.; K6bel, J.; Gendy, C.; Lee, L. M.; Jenkins, H.; Britten, J. F.; Morim, D. R.; et al. Supramolecular macrocycles reversibly assembled by Te(...)O chalcogen bonding. *Nat. Commun.* **2016**, *7*, 11299.
- (32) Werz, D. B.; Gleiter, R.; Rominger, F. Nanotube formation favored by chalcogen-chalcogen interactions. *J. Am. Chem. Soc.* **2002**, *124*, 10638–10639.
- (33) Zahn, S.; Frank, R.; Hey-Hawkins, E.; Kirchner, B. Pnicogen bonds: A new molecular linker? *Chem. - Eur. J.* **2011**, *17*, 6034–6038.
- (34) Cozzolino, A. F.; Yang, Q.; Vargas-Baca, I. Engineering second-order nonlinear optical activity by means of a noncentrosymmetric distortion of the [Te-N]₂ supramolecular synthon. *Cryst. Growth Des.* **2010**, *10*, 4959–4964.
- (35) Beno, B. R.; Yeung, K.-S.; Bartberger, M. D.; Pennington, L. D.; Meanwell, N. A. A. Survey of the role of noncovalent sulfur interactions in drug design. *J. Med. Chem.* **2015**, *58*, 4383–4438.
- (36) Nagao, Y.; Hirata, T.; Goto, S.; Sano, S.; Kakehi, A.; Iizuka, K.; Shiro, M. Intramolecular nonbonded S...O interaction recognized in (acylimino)thiadiazoline derivatives as angiotensin II receptor antagonists and related compounds. *J. Am. Chem. Soc.* **1998**, *120*, 3104–3110.
- (37) Cavallo, G.; Metrangolo, P.; Pilati, T.; Resnati, G.; Sansotera, M.; Terraneo, G. Halogen bonding: A general route in anion recognition and coordination. *Chem. Soc. Rev.* **2010**, *39*, 3772–3783.
- (38) Mahmudov, K. T.; Kopylovich, M. N.; Guedes da Silva, M. F. C.; Pombeiro, A. J. L. Chalcogen bonding in synthesis, catalysis and design of materials. *Dalton Trans.* **2017**, *46*, 10121–10138.
- (39) Gilday, L. C.; Robinson, S. W.; Barendt, T. A.; Langton, M. J.; Mullaney, B. R.; Beer, P. D. Halogen Bonding in Supramolecular Chemistry. *Chem. Rev.* **2015**, *115*, 7118–7195.
- (40) Ho, P. In *Halogen bonding I*; Metrangolo, P., Resnati, G., Eds.; Topics in current chemistry; Springer International Publishing: Berlin, 2015; Vol. 358, pp 241–276.
- (41) Xu, Z.; Yang, Z.; Liu, Y.; Lu, Y.; Chen, K.; Zhu, W. Halogen bond: Its role beyond drug-target binding affinity for drug discovery and development. *J. Chem. Inf. Model.* **2014**, *54*, 69–78.
- (42) Jentzsch, A. V.; Matile, S. In *Halogen bonding I*; Metrangolo, P., Resnati, G., Eds.; Topics in current chemistry; Springer International Publishing: Berlin, 2015; Vol. 358, pp 205–239.
- (43) Zordan, F.; Brammer, L.; Sherwood, P. Supramolecular chemistry of halogens: Complementary features of inorganic (M-X) and organic (C-X) halogens applied to M-X...X-C halogen bond formation. *J. Am. Chem. Soc.* **2005**, *127*, 5979–5989.
- (44) Podsiadlo, M.; Olejniczak, A.; Katrusiak, A. Halogen...halogen contra C-H...halogen interactions. *CrystEngComm* **2014**, *16*, 8279–8285.
- (45) Tothadi, S.; Joseph, S.; Desiraju, G. R. Synthron modularity in cocrystals of 4-bromobenzamide with n-alkanedicarboxylic acids: Type I and type II halogen...halogen interactions. *Cryst. Growth Des.* **2013**, *13*, 3242–3254.
- (46) Mukherjee, A.; Desiraju, G. R. Halogen bonds in some dihalogenated phenols: Applications to crystal engineering. *IUCrJ* **2014**, *1*, 49–60.
- (47) Sakurai, T.; Sundaralingam, M.; Jeffrey, G. A. A nuclear quadrupole resonance and X-ray study of the crystal structure of 2,5-dichloroaniline. *Acta Crystallogr.* **1963**, *16*, 354–363.
- (48) Desiraju, G. R.; Parthasarathy, R. The nature of σ^* halogen...halogen interactions: Are short halogen contacts due to specific attractive forces or due to close packing of nonspherical atoms? *J. Am. Chem. Soc.* **1989**, *111*, 8725–8726.
- (49) Duarte, D. J. R.; Peruchena, N. M.; Alkorta, I. Double hole-lump interaction between halogen atoms. *J. Phys. Chem. A* **2015**, *119*, 3746–3752.
- (50) Capdevila-Cortada, M.; Castello, J.; Novoa, J. J. The nature of the C-Cl...Cl-C intermolecular interactions found in molecular crystals: A general theoretical-database study covering the 2.75–4.0 Å range. *CrystEngComm* **2014**, *16*, 8232–8242.
- (51) Awwadi, F. F.; Willett, R. D.; Peterson, K. A.; Twamley, B. The nature of halogen...halogen synthons: Crystallographic and theoretical studies. *Chem. - Eur. J.* **2006**, *12*, 8952–8960.
- (52) Metrangolo, P.; Resnati, G. Type II halogen...halogen contacts are halogen bonds. *IUCrJ* **2014**, *1*, 5–7.
- (53) Reddy, C. M.; Kirchner, M. T.; Gundakaram, R. C.; Padmanabhan, K. A.; Desiraju, G. R. Isostructurality, polymorphism and mechanical properties of some hexahalogenated benzenes: The nature of halogen...halogen interactions. *Chem. - Eur. J.* **2006**, *12*, 2222–2234.
- (54) Setiawan, D.; Kraka, E.; Cremer, D. Strength of the pnicogen bond in complexes involving group Va elements N, P, and As. *J. Phys. Chem. A* **2015**, *119*, 1642–1656.
- (55) Setiawan, D.; Cremer, D. Super-pnicogen bonding in the radical anion of the fluorophosphine dimer. *Chem. Phys. Lett.* **2016**, *662*, 182–187.
- (56) Antonijevic, I. S.; Janjic, G. V.; Milcic, M. K.; Zaric, S. D. Preferred geometries and energies of sulfur-sulfur interactions in crystal structures. *Cryst. Growth Des.* **2016**, *16*, 632–639.
- (57) Shukla, R.; Chopra, D. Crystallographic and theoretical investigation on the nature and characteristics of type I C-S...S-C interactions. *Cryst. Growth Des.* **2016**, *16*, 6734–6742.
- (58) Del Bene, J. E.; Sanchez-Sanz, G.; Alkorta, I.; Elguero, J. Homo- and heterochiral dimers (PHFX)₂, X = Cl, CN, CH₃, NC: To what extent do they differ? *Chem. Phys. Lett.* **2012**, *538*, 14–18.
- (59) Del Bene, J. E.; Alkorta, I.; Elguero, J. Substituent effects on the properties of pnicogen-bonded complexes H₂XP:PYH₂, for X, Y = F, Cl, OH, NC, CCH, CH₃, CN, and H. *J. Phys. Chem. A* **2015**, *119*, 224–233.
- (60) Trujillo, C.; S6nchez-Sanz, G.; Alkorta, I.; Elguero, J. Halogen, chalcogen and pnicogen interactions in (XNO₂)₂ homodimers (X = F, Cl, Br, I). *New J. Chem.* **2015**, *39*, 6791–6802.

- (61) Bleiholder, C.; Werz, D. B.; Köppel, H.; Gleiter, R. Theoretical investigations on chalcogen-chalcogen interactions: What makes these nonbonded interactions bonding? *J. Am. Chem. Soc.* **2006**, *128*, 2666–2674.
- (62) Bleiholder, C.; Gleiter, R.; Werz, D. B.; Köppel, H. Theoretical investigations on heteronuclear chalcogen-chalcogen interactions: On the nature of weak bonds between chalcogen centers. *Inorg. Chem.* **2007**, *46*, 2249–2260.
- (63) Azofra, L. M.; Alkorta, I.; Scheiner, S. Chalcogen bonds in complexes of SOXY (X, Y = F, Cl) with nitrogen bases. *J. Phys. Chem. A* **2015**, *119*, 535–541.
- (64) Alkorta, I.; Elguero, J.; Del Bene, J. E. Characterizing traditional and chlorine-shared halogen bonds in complexes of phosphine derivatives with ClF and Cl₂. *J. Phys. Chem. A* **2014**, *118*, 4222–4231.
- (65) Del Bene, J. E.; Alkorta, I.; Elguero, J. Influence of substituent effects on the formation of P...Cl pnictogen bonds or halogen bonds. *J. Phys. Chem. A* **2014**, *118*, 2360–2366.
- (66) Shukla, R.; Chopra, D. Pnictogen bonds or chalcogen bonds: Exploiting the effect of substitution on the formation of P...Se noncovalent bonds. *Phys. Chem. Chem. Phys.* **2016**, *18*, 13820–13829.
- (67) Møller, C.; Plesset, M. S. Note on an approximation treatment for many-electron systems. *Phys. Rev.* **1934**, *46*, 618–622.
- (68) Steinmann, S. N.; Piemontesi, C.; Delachat, A.; Corminboeuf, C. Why are the interaction energies of charge-transfer complexes challenging for DFT? *J. Chem. Theory Comput.* **2012**, *8*, 1629–1640.
- (69) Bauzá, A.; Alkorta, I.; Frontera, A.; Elguero, J. On the reliability of pure and hybrid DFT methods for the evaluation of halogen, chalcogen, and pnictogen bonds involving anionic and neutral electron donors. *J. Chem. Theory Comput.* **2013**, *9*, 5201–5210.
- (70) Kozuch, S.; Martin, J. M. L. Halogen bonds: Benchmarks and theoretical analysis. *J. Chem. Theory Comput.* **2013**, *9*, 1918–1931.
- (71) Raghavachari, K.; Trucks, G. W.; Pople, J. A.; Head-Gordon, M. A fifth-order perturbation comparison of electron correlation theories. *Chem. Phys. Lett.* **1989**, *157*, 479–483.
- (72) Rezac, J.; Hobza, P. Describing noncovalent interactions beyond the common approximations: How accurate is the "Gold Standard," CCSD(T) at the complete basis set limit? *J. Chem. Theory Comput.* **2013**, *9*, 2151–2155.
- (73) Brauer, B.; Kesharwani, M. K.; Kozuch, S.; Martin, J. M. L. The S66 × 8 benchmark for noncovalent interactions revisited: Explicitly correlated ab initio methods and density functional theory. *Phys. Chem. Chem. Phys.* **2016**, *18*, 20905–20925.
- (74) Rezac, J.; Hobza, P. Benchmark calculations of interaction energies in noncovalent complexes and their applications. *Chem. Rev.* **2016**, *116*, 5038–5071.
- (75) Hill, J. G.; Hu, X. Theoretical insights into the nature of halogen bonding in prereactive complexes. *Chem. - Eur. J.* **2013**, *19*, 3620–3628.
- (76) Oliveira, V.; Kraka, E.; Cremer, D. The intrinsic strength of the halogen bond: Electrostatic and covalent contributions described by coupled cluster theory. *Phys. Chem. Chem. Phys.* **2016**, *18*, 33031–33046.
- (77) Woon, D.; Dunning, T. J. Gaussian basis sets for use in correlated molecular calculations. IV. Calculation of static electrical response properties. *J. Chem. Phys.* **1994**, *100*, 2975–2988.
- (78) Dunning, T. Gaussian basis sets for use in correlated molecular calculations. I. The atoms boron through neon and hydrogen. *J. Chem. Phys.* **1989**, *90*, 1007–1023.
- (79) Woon, D.; Dunning, T. Gaussian basis sets for use in correlated molecular calculations. III. The atoms aluminum through argon. *J. Chem. Phys.* **1993**, *98*, 1358–1371.
- (80) Konkoli, Z.; Cremer, D. A new way of analyzing vibrational spectra I. Derivation of adiabatic internal modes. *Int. J. Quantum Chem.* **1998**, *67*, 1–11.
- (81) Cremer, D.; Larsson, J. A.; Kraka, E. In *Theoretical and Computational Chemistry, Vol. 5, Theoretical Organic Chemistry*; Parkanyi, C., Ed.; Elsevier: Amsterdam, 1998; pp 259–327.
- (82) Zou, W.; Kalescky, R.; Kraka, E.; Cremer, D. Relating normal vibrational modes to local vibrational modes with the help of an adiabatic connection scheme. *J. Chem. Phys.* **2012**, *137*, 084114.
- (83) Zou, W.; Cremer, D. Properties of local vibrational modes: The infrared intensity. *Theor. Chem. Acc.* **2014**, *133*, 1451.
- (84) Wilson, E. B.; Decius, J. C.; Cross, P. C. *Molecular vibrations. The theory of infrared and Raman vibrational spectra*; McGraw-Hill: New York, 1955.
- (85) Zou, W.; Cremer, D. C₂ in a box: Determining its intrinsic bond strength for the X¹Σ_g⁺ ground state. *Chem. - Eur. J.* **2016**, *22*, 4087–4089.
- (86) Kraka, E.; Larsson, J. A.; Cremer, D. In *Computational spectroscopy: Methods, experiments and applications*; Grunenberg, J., Ed.; Wiley: New York, 2010; pp 105–149.
- (87) Boys, S.; Bernardi, F. The calculation of small molecular interactions by the differences of separate total energies. Some procedures with reduced errors. *Mol. Phys.* **1970**, *19*, 553–566.
- (88) Mentel, L. M.; Baerends, E. J. Can the counterpoise correction for basis set superposition effect be justified? *J. Chem. Theory Comput.* **2014**, *10*, 252–267.
- (89) van Duijneveldt, F. B.; van Duijneveldt-van de Rijdt, J. G. C. M.; van Lenthe, J. H. State of the art in counterpoise theory. *Chem. Rev.* **1994**, *94*, 1873–1885.
- (90) Riplinger, C.; Neese, F. An efficient and near linear scaling pair natural orbital based local coupled cluster method. *J. Chem. Phys.* **2013**, *138*, 034106.
- (91) Riplinger, C.; Sandhoefer, B.; Hansen, A.; Neese, F. Natural triple excitations in local coupled cluster calculations with pair natural orbitals. *J. Chem. Phys.* **2013**, *139*, 134101.
- (92) Dunning, T. J. Gaussian basis sets for use in correlated molecular calculations I. The atoms boron through neon and hydrogen. *J. Chem. Phys.* **1989**, *90*, 1007–1023.
- (93) Cremer, D.; Kraka, E. A description of the chemical bond in terms of local properties of electron density and energy. *Croat. Chem. Acta* **1984**, *57*, 1259–1281.
- (94) Cremer, D.; Kraka, E. Chemical bonds without bonding electron density - Does the difference electron density analysis suffice for a description of the chemical bond? *Angew. Chem., Int. Ed. Engl.* **1984**, *23*, 627–628.
- (95) Kraka, E.; Cremer, D. In *Theoretical models of chemical bonding. The concept of the chemical bond*, Vol. 2; Maksic, Z., Ed.; Springer Verlag: Heidelberg, Germany, 1990; pp 453–542.
- (96) Clark, T. Halogen bonds and σ-holes. *Faraday Discuss.* **2017**, *203*, 9–27.
- (97) Murray, J. S.; Politzer, P. Molecular electrostatic potentials and noncovalent interactions. *WIREs Comput. Mol. Sci.* **2017**, *7*, e1326.
- (98) Weinhold, F.; Landis, C. R. *Valency and bonding: A natural bond orbital donor-acceptor perspective*; Cambridge University Press: Cambridge, U.K., 2003.
- (99) Chai, J. D.; Head-Gordon, M. Long-range corrected hybrid density functionals with damped atom-atom dispersion corrections. *Phys. Chem. Chem. Phys.* **2008**, *10*, 6615.
- (100) Chai, J. D.; Head-Gordon, M. Systematic optimization of long-range corrected hybrid density functionals. *J. Chem. Phys.* **2008**, *128*, 084106.
- (101) Stone, A. J. Natural bond orbitals and the nature of the hydrogen bond. *J. Phys. Chem. A* **2017**, *121*, 1531–1534.
- (102) Kraka, E.; Zou, W.; Filatov, M.; Grafenstein, J.; Izotov, D.; Gauss, J.; He, Y.; Wu, A.; Konkoli, Z.; Polo, V.; et al. *COLOGNE2016*; 2016; see <http://www.smu.edu/catco> (accessed Nov 10, 2017).
- (103) Stanton, J. F.; Gauss, J.; Harding, M. E.; Szalay, P. G. *CFOUR, A quantum chemical program package*, 2010; see <http://www.cfour.de> (accessed Nov 10, 2017).
- (104) Keith, T. *TK Gristmill Software (aim.tkgristmill.com)*, 2011; Overland Park, KS, USA.
- (105) Zou, W.; Nori-Shargh, D.; Boggs, J. E. On the covalent character of rare gas bonding interactions: A new kind of weak interaction. *J. Phys. Chem. A* **2013**, *117*, 207–212.

- (106) Lu, T.; Chen, F. Multiwfn: A multifunctional wavefunction analyzer. *J. Comput. Chem.* **2012**, *33*, 580–592.
- (107) Setiawan, D.; Kalescky, R.; Kraka, E.; Cremer, D. Direct measure of metal-ligand bonding replacing the Tolman electronic parameter. *Inorg. Chem.* **2016**, *55*, 2332–2344.
- (108) Kraka, E.; Setiawan, D.; Cremer, D. Re-evaluation of the bond length-bond strength rule: The stronger bond is not always the shorter bond. *J. Comput. Chem.* **2016**, *37*, 130–142.
- (109) Clark, T. Polarization, donor-acceptor interactions, and covalent contributions in weak interactions: A clarification. *J. Mol. Model.* **2017**, *23*, 297.